IOP Publishing
Plasma Physics and Controlled Fusion
Plasma Phys. Control. Fusion 60 (2018) 044013 (8pp)
https://doi.org/10.1088/1361-6587/aaabfd

Probing plasma wakefields using electron bunches generated from a laser wakefield accelerator

C J Zhang[1,2], Y Wan[1], B Guo[1], J F Hua[1], C-H Pai[1], F Li[1], J Zhang[1], Y Ma[1], Y P Wu[1], X L Xu[2,3], W B Mori[2,3], H-H Chu[4], J Wang[4,5,6], W Lu[1] and C Joshi[2]

[1] Department of Engineering Physics, Tsinghua University, Beijing 100084, People's Republic of China
[2] Department of Electrical Engineering, University of California Los Angeles, Los Angeles, CA 90095, United States of America
[3] Department of Physics and Astronomy, University of California Los Angeles, Los Angeles, CA 90095, United States of America
[4] Department of Physics, National Central University, Jhong-Li 32001, Taiwan
[5] Institute of Atomic and Molecular Sciences, Academia Sinica, Taipei 10617, Taiwan
[6] Department of Physics, National Taiwan University, Taipei 10617, Taiwan

E-mail: jfhua@tsinghua.edu.cn

Received 1 December 2017, revised 25 January 2018
Accepted for publication 31 January 2018
Published 1 March 2018

Abstract

We show experimental results of probing the electric field structure of plasma wakes by using femtosecond relativistic electron bunches generated from a laser wakefield accelerator. Snapshots of laser-driven linear wakes in plasmas with different densities and density gradients are captured. The spatiotemporal evolution of the wake in a plasma density up-ramp is recorded. Two parallel wakes driven by a laser with a main spot and sidelobes are identified in the experiment and reproduced in simulations. The capability of this new method for capturing the electron- and positron-driven wakes is also shown via 3D particle-in-cell simulations.

Keywords: laser wakefield accelerator, plasma, wakefield structure, electron probe

(Some figures may appear in colour only in the online journal)

1. Introduction

The interaction of intense lasers or charged particle beams with plasma can induce extremely strong electric [1, 2] and magnetic fields [3]. Such fields are relevant to many important physical phenomena ranging from acceleration [1, 2] to inertial confinement fusion [4]. For example, intense lasers or charged particle beams can excite plasma wakes through their ponderomotive force or Coulomb force which travel at nearly the speed of light. The electric fields inside such wakes are so strong that can be used to accelerate electrons [5–14] or positrons [15, 16] much more rapidly than using a conventional radio-frequency based accelerator. Extensive studies [10, 12–14, 16–19] have been carried out to show the potential of plasma-based accelerators in approaching to the building of plasma-based linear colliders [20] and the attractive applications in building compact beam/light sources [18, 19, 21, 22].

One of the challenging problems needs to solve is the direct probing of the field structure of plasma wakes. In order to understand important physical processes such as injection [23–25] and beam loading [26–29] and to optimise plasma-based accelerators, one needs information of the wakefield structures. However, in a plasma-based accelerator, the wake propagates with its phase velocity equals to the group velocity of the driver which is very close to the speed of light, c. This makes probing of the wakefield structure difficult by requiring the use of extremely short probe pulses, no matter what kind of probe is used. It is because the front part and the back part of the probe will see different phases of the wake since the wake is moving at the speed of light. As a consequence, the length of the probe should be much shorter than the plasma wavelength to minimize the effect induced by the relativistic motion of the wake. Therefore, although long-pulse (∼ps) charged particle beams including electron [30, 31] and proton beams [3, 32] have been used to diagnose field structures generated in laser–plasma interactions, they are not suitable for probing relativistic plasma wakes. Betatron oscillation of the high-energy drive beam itself has also been used to retrieve the longitudinal field structure of a nonlinear plasma accelerator cavity [33]. However, this method gives only the field structure averaged over the whole accelerating length.

Very recently, we have demonstrated a method to solve this challenging problem—probing the wakefield structures of a laser-driven wake by using a femtosecond relativistic electron bunch generated from another laser wakefield accelerator (LWFA) [34]. Using electron beams as a probe is attractive because they can capture the field structures directly. Since the electric field structures instead of only the density structures are probed, this new technique may reveal more useful information in addition to that obtained by optical methods such as frequency-domain interferometry [35, 36] and ultrafast shadowgraphy [37, 38]. In principle, there is no limitation on using electron bunches generated from either a conventional RF-based accelerator or a plasma-based accelerator. However, it is not easy to compress the bunch from a conventional RF-based accelerator down to few femtoseconds so that the bunch is suitable for probing wakes excited in relatively high-density plasmas (10^{18}–10^{19} cm^{-3}). In contrast, electron bunches generated from an LWFA are extremely short [39–41] and highly relativistic (with the Lorentz factor $\gamma \gg 1$), therefore can freeze the light-speed-moving wakes. Also, these electron bunches are usually well synchronized with the drive laser, which could be easily synchronized with the laser driving the wakes that being probed. Due to their extremely high accelerating gradients, LWFAs are very compact which means in principle multiple beams can be used to diagnose the same wake from different angles and/or time delays to obtain extra information in a single-shot measurement. Therefore, LWFA generated electron bunches can be used as a perfect tool for capturing wakefield structures.

Soon after the concept of LWFA was proposed, beam-driven plasma wakefield accelerator (PWFA) was also proposed [2]. By using high-energy charged-particle beams as a driver, PWFA has attractive advantages. The dephasing length is much longer than that of an LWFA because the phase velocity of plasma waves driven by a beam driver is usually much larger than that driven by a laser driver. The evolution scale length of the beam driver is characterized by the betatron motion wavelength, which can also be much larger than the Rayleigh length of an intense laser pulse currently used in most experiments [19]. Both of these features are beneficial to greatly increase the energy gain of the accelerated beam. Many important results have been reported, including the acceleration of electrons over a metre length and high-quality, high-efficiency acceleration of both electrons and positrons [8–10, 15, 16]. These results are paving the way towards building plasma-based colliders. In order to understand the relevant physics, it is necessary to have a direct diagnosis of wakefield structures of both electron- and positron-driven wakes. Similar to the probing of laser-driven wakes, LWFA generated electron bunches can also be used to probe these beam-driven wakes. Although it may require a more sophisticated synchronization than that in the laser-driven case, the applicability of the method to probing beam-driven wakes is worth exploring because there is no existing technique that can measure the instantaneous field distribution of beam-driven wakes, especially in low-density plasmas.

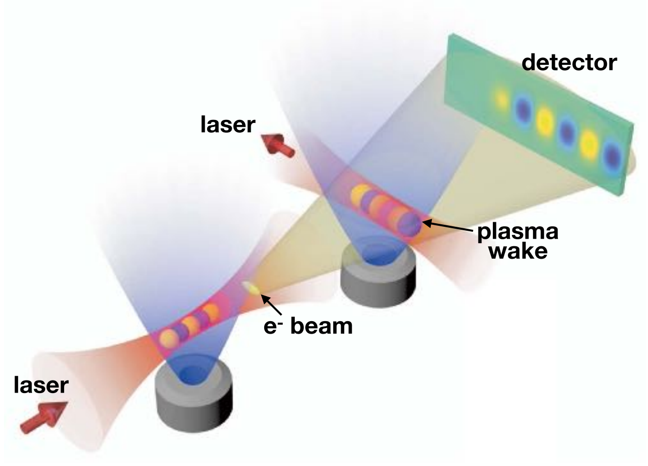

Figure 1. The schematic drawing of using a relativistic electron bunch to probe a laser-driven plasma wakefield.

In this paper, experimental results of probing laser-driven wakes are presented. The electric field structure of linear wakes driven in plasmas with different densities and density gradients are captured. The spatiotemporal evolution of the wake in a plasma density up-ramp is recorded. Despite a fast-evolving feature of the wake, the initial profile of the low-density plasma is reconstructed. In the experiment, parallel wakes excited by a laser with a main spot and sidelobes are identified from the snapshot captured by the probe beam. In the last part, we also show particle-in-cell (PIC) simulation results where the method is used to capture the field structures in beam-driven wakes.

2. Experimental and simulation results

2.1. Probing wakefield structures of a laser-driven wake

The schematic drawing of the concept of using a relativistic electron bunch to probe a laser-driven plasma wakefield is shown in figure 1. Electron bunches with peak energy ranging from tens of MeV to several GeV can be generated by using an ultrashort laser with peak power varying from several TW to a few PW interacting with plasmas [12–14]. These electrons then traverse through a second wake driven by the second laser at the right angle after an adjustable time delay. This can be achieved by simply adjusting the delay between the two laser pulses because the electron bunch is usually well synchronized with the first drive laser. The intense electric fields in the wake being detected will act like microlens to focus or defocus different parts the probe beam. In other words, the transverse momentum of the probe electrons will

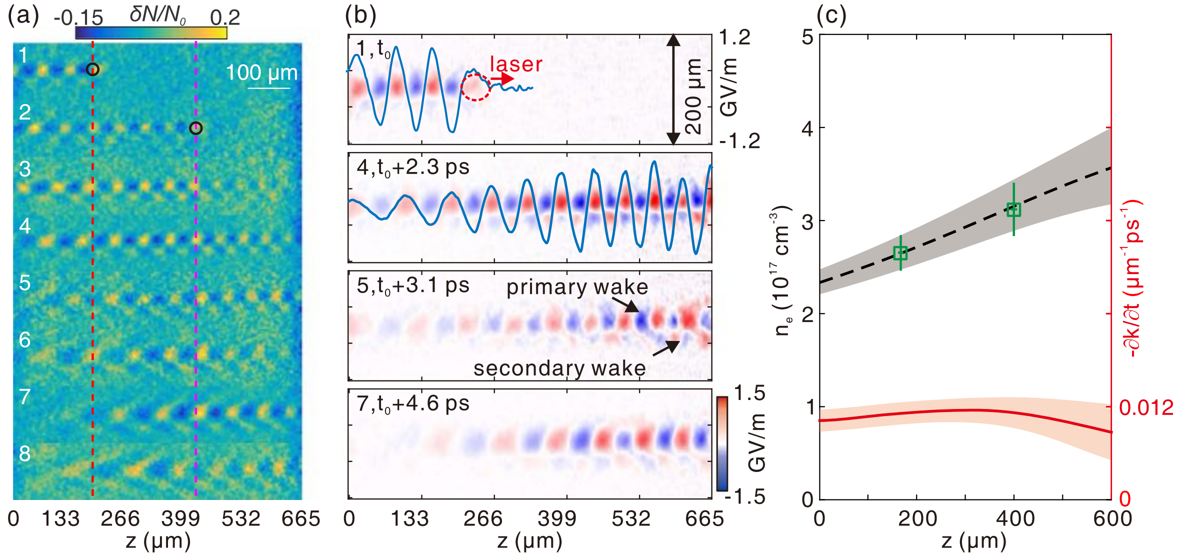

Figure 2. Snapshots of wakes, reconstructed accelerating fields and initial density profile of the plasma up-ramp. (a) A series of snapshots of wakes propagating in a density up-ramp. The time delay between sequential frames is 0.77 ps. In the top two frames, the black circles mark the position of the centre of the first wake period. (b) Reconstructed accelerating fields for four representative snapshots in (a). Axial lineouts of the reconstructed field are also shown in the first two frames. (c) Retrieved initial density profile of the plasma up-ramp (dashed black line) and the local gradient of the plasma frequency $\partial\omega_p/\partial z = -\partial k/\partial t$ (red line). The green squares show the plasma density calculated using the wavelength of the first plasma period at locations marked by the black circles in (a).

be modulated by the wakefield. As a result, density modulations will appear after the probe beam keeps propagating for a short distance (a few mm to several cm depending on the beam and wake parameters). As had been shown in [42], by measuring these density modulations we can get clear snapshots of the wake and then retrieve the electric field distributions in both the longitudinal and the transverse directions in a single shot. We note that the field distributions can be quantitatively retrieved for linear wakes and qualitatively retrieved for nonlinear wakes [42].

The setup and the detailed parameters for the laser, plasma and electron beams used in the experiment can be found in [34]. Here we summarize the key parameters for the convenience of the reader. The peak energy of the LWFA-generated electron bunch is about 70 MeV with an FWHM spread of ~15% and a root-mean-square (rms) divergence of 2 mrad. The charge contained in the peak is ~5 pC. The pulse length of the probe beam was measured to be 1.8 fs (rms) using the method in [40]. After being generated, the probe beam propagates in vacuum for 11 cm and then traverses through the second wake driven by another laser ($a_0 \sim 0.26$) in the second gas jet with a 3 mm diameter. The plasma density is set to $\sim 10^{17}$ cm^{-3} by using a very low backing pressure and by increasing the distance between the nozzle exit and the second laser beam to several mm. After traversing through the second wake, the probe beam keeps propagating in vacuum for another 42 cm to let the transverse momentum modulations induced by the second wake evolve into density modulations. These density modulations are then recorded by an imaging system consisting of a ~100 μm YAG:Ce screen, a pair of relay lenses (spatial resolution calibrated to be 2.8 μm) and an electron multiplying charge-coupled device.

Figure 2(a) shows the recorded density modulation of the probe beam, which can be seen as snapshots of the wake that being probed. Note that normalized density modulations $\delta N/N_0$ are shown in these plots, where N_0 is the background density of the unperturbed probe and $\delta N = N - N_0$ is the difference between the measured density and the background density. Here N_0 is obtained by smoothing the measured density profile of the probe to remove the modulations induced by the wakefield. By varying the time delay between the two laser pulses, a series of snapshots with an interval of 0.77 ps are captured. In the top two frames, the centres of the first wake period right after the drive laser pulse are marked by black circles. The plasma density at these locations can be calculated from the wavelength of the wake through $n_p = \frac{\epsilon_0 m_e}{e^2}\left(\frac{2\pi c}{\lambda_p}\right)^2$ since there is not enough time for the wake to evolve. Here λ_p is the measured plasma wavelength. The calculated densities at these two positions are 2.7×10^{17} cm^{-3} and 3.1×10^{17} cm^{-3}, respectively. Dividing the distance between these two circles by the time delay of 0.77 ps gives the propagating speed of the wake, which is the speed of light as expected because in such a low-density plasma the phase velocity of the linear wake $v_\phi = c\sqrt{1 - n_p/n_c}$ should be very close to c. Here n_p is the plasma density and $n_c = m_e \epsilon_0 \omega_0^2/e^2$ is the critical density. In the third and the following frames, the laser has propagated out of the view. In each of these frames, one can clearly see that the wavelength of the wake decreases from left to right, which indicates that there may exist a density up-ramp. However, as we will discuss later, the initial profile of this density up-ramp cannot be calculated directly from the wake wavelength using the aforementioned formula because the wake may have evolved. The wavelength of the wake increases with time at a fixed location (e.g. the locations marked by the vertical dashed lines) provides us with a hint that the wake is evolving because such a significant increase in wavelength is not likely to be caused by the density drop due to plasma expansion in less than 5 ps.

The distribution of electric fields in these linear wakes can be retrieved from the measured density modulations of the probe beam [34, 42]. The retrieved fields are shown in figure 2(b). For simplicity, here we only show the reconstructed E_z fields because the E_r fields are related to the corresponding E_z fields through the Panofsky–Wenzel theorem, $\partial E_z/\partial r = \partial(E_r - B_\theta)/\partial z$ [43], with the B_θ term negligible compared with the E_r term. For the same reason, only the results for four representative frames are shown. In the first two frames in figure 2(b), axial lineouts are overlaid on top of the 2D distribution of E_z. The peak amplitude of reconstructed E_z is about 1 GV/m due to the low plasma density and the low laser intensity used in this experiment. The results agree well with PIC simulations as shown in [34].

One may have noticed an interesting feature of the E_z fields in figure 2(b)—there is a small secondary wake alongside the primary wake. More interestingly, the secondary wake is about π rad shifted in phase with respect to the primary wake. It turned out that this phenomenon is caused by the non-ideal incident laser with a main spot and sidelobes in its intensity profile which we will discuss later.

In figure 2(c), we show the retrieved initial profile of the density up-ramp by the black dashed line. The green dots mark the densities calculated using the wavelength of the first plasma period at locations indicated by the black circles in figure 1(a). As we have explained, the densities at these two locations represent the real initial density because the wakes have no time to evolve. The error bars arise from the uncertainty in determining the wavelength through the wavelet transform. Since the wake evolves with time after it has been excited and the wavelength of the wake changes with time, in general, we cannot calculate the density directly from the measured wavelength. However, as shown in [34, 44], we found out that the wake evolves in such a way that the change of wavenumber at a given location as a function of time can be related to the local frequency gradient, i.e., $\partial k/\partial t = -\partial\omega_p/\partial z$. This change in the wake wavenumber happens at every z location as time passes. Therefore, for each location, we can calculate the local wavenumber $k(z, t) = 2\pi/\lambda(z)$ for every single frame in figure 2(a), where t is the time starting from when the wake is excited. In other words, for each location z, we can get k as a function of t and by fitting a linear line to these $(t_i, k(t_i))$ points to get the slope, i.e., $\partial k/\partial t$. A linear fit to the data is used under the assumption that the density profile does not change in the very short time period (<5 ps) during the experiment so that $\partial\omega_p/\partial z$ is constant in time. The calculated $-\partial k/\partial t$ for different z locations are shown as the red line in figure 2(c). The shaded area represents the 95% percent confidence interval of the linear fitting. Since now we have in hand both the gradient $\partial\omega_p/\partial z$ and the two values of ω_p at locations marked by the black circles in figure 2(a) as boundary conditions, the whole profile of the initial density up-ramp can be retrieved as shown by the dashed black line. We use $\omega_p(z = 170\ \mu\text{m})$ as the boundary condition to retrieve the density profile and ω_p at $z = 400\ \mu$m as a cross-checking point, namely, it should locate on the retrieved density profile which is exactly the case shown in figure 2(c).

The retrieved profile shows that there is indeed a density up-ramp as we have inferred from the snapshots in figure 2(a). In the measured region of the 3 mm jet as shown in figure 2, the plasma density increases from 2.3×10^{17} to 3.5×10^{17} cm^{-3}. Such a low density is very difficult to measure using existing techniques like interferometry. However, this new diagnostic tool shows its capability to characterize very low-density plasmas suitable for building single-stage 10 GeV LWFAs [17]. Unlike the linear dependence of the refractive index on the plasma density ($\eta = 1 - n_p/2n_c$, with relativistic corrections neglected. η is refractive index, n_p is plasma density and n_c is the critical plasma density), the electric field in the wake scales with the square root of the plasma density, $E_z \propto \sqrt{n_p}$ [19], which changes more slowly as the density drops. More importantly, even in very low-density plasmas, the amplitude of the wakefield can still be as large as GeV/m, strong enough to deflect the probe electrons to form a snapshot of the wake. Therefore, this new method can hopefully work in even lower-density plasmas than that presented in this paper.

In the experiment, we changed the plasma density by varying the backing pressure while keeping the laser parameters unchanged. The delay between the two laser pulses was fixed to $t_0 + 3$ ps and the camera was set to record the same region as in figure 2(a), i.e., the rising edge of the gas jet. Here t_0 is the time when the first frame in figure 2(a) was taken. We also tried to measure the wakes in the uniform (central) region of the plasma, however, the density was too high so that we did not get a snapshot with clear wake structures in that case. The measured wake snapshots are shown in figures 3(a)–(e) with increasing plasma densities. The corresponding axial lineouts of the measured density modulation are shown in (f)–(j). It can be clearly seen that the wavelength of the wake decreases as the plasma density increases. The amplitude of the measured density modulation also drops as the density increases, but it is due to the emittance of the probe beam as had been discussed in [42]. In figure 3(k) we show the calculated density as a function of the backing pressure. The densities are calculated using the wavelength of the wake at $z \approx 400\ \mu$m. The delay between the two laser pulses is 3 ps for these snapshots, therefore the time delay between the drive laser and the wake at $z \approx 400\ \mu$m is 2.4 ps. Consequently, we note that these densities could be ~30% lower than the real values because the wake wavelength may have evolved a little bit after ~2 ps from being excited due to the aforementioned reason. However, the measured densities still increase linearly as a function of the backing pressure.

2.2. Probing two parallel plasma wakes

In experiments, an imperfect laser pulse can drive asymmetric wakes. Specifically, if the laser pulse consists of parallel sub-

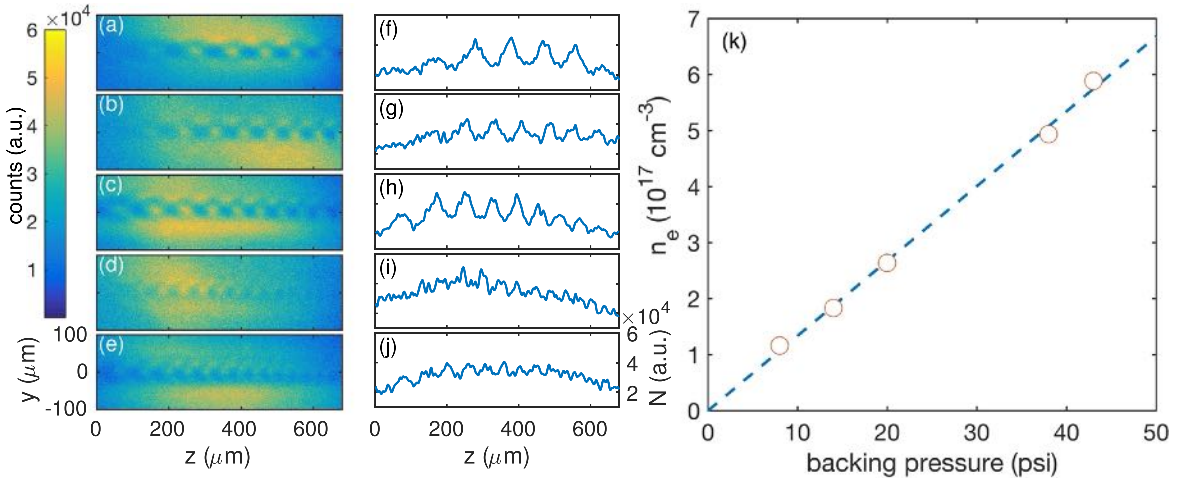

Figure 3. Wakes in plasmas with different densities. (a)–(e) Snapshots of wakes in plasmas with increasing density. (f)–(j) Axial lineouts of the corresponding snapshots. (k) Open circles show the calculated densities at $z \approx 400\ \mu$m as a function of backing pressure. The dashed line is the best linear fit to the data.

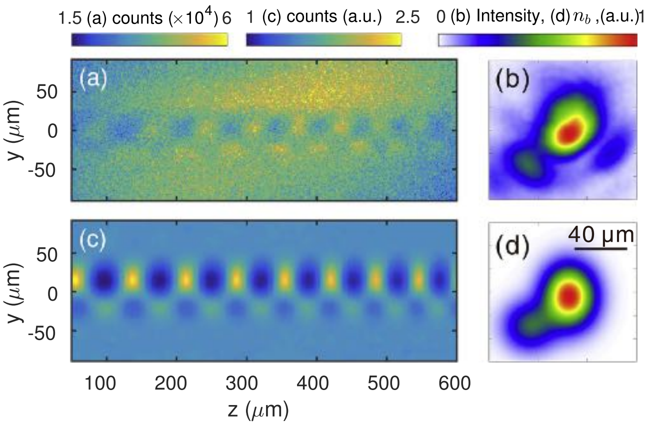

Figure 4. Snapshots of two parallel wakes. (a) Snapshot of two parallel wakes obtained in the experiment. A weaker secondary wake can be found beside the stronger primary wake. (b) The laser intensity profile measured at $z \approx 0$ shows a main spot and sidelobes. (c) Simulated snapshot of parallel wakes excited by two beam drivers as shown in (d).

pulses, it can excite multi-parallel wakes, which may be used to generate high-charge electron beams [45]. Such parallel wakes are observed in the experiment as shown in figures 2(a) and (b). In all frames in figure 2(b), one can see that there is a small secondary wake alongside the primary wake. We have mentioned that this can be possibly explained by that these wakes are excited by the imperfect laser pulse with a main spot and sidelobes in its intensity profile. This is verified by 3D PIC simulations in this section.

The unnormalized original density profile of the probe of the same shot corresponding to the fourth frame in figure 2(a) is replotted in figure 4(a). Figure 4(b) shows the laser intensity profile measured at the $z \approx 0$ position in figure 4(a). In addition to the bright central spot, there appear to be either two weaker spots or part of a ring around the main spot arising from aberrations. Apparently, the intensity of the weaker feature is nevertheless sufficient to drive the weaker second wake beside the primary wake. The two wakes are separated vertically by a distance that is the same as the vertical separation of the laser spots. The two laser spots are also separated along the propagation direction of the probe, which introduces a phase shift between the images of the two wakes. This is because the probe captures the primary wake first and then samples the secondary wake but at a different phase since both wakes have moved forward. Both the vertical separation and the phase shift between the images of the two wakes can be clearly seen in figure 4(a).

This hypothesis is confirmed in figure 4(c) by 3D PIC simulations. To save simulation time, the measured laser intensity profile is approximated by two electron beam drivers, with properly scaled amplitudes, widths and separations. The simulation box is $920 \times 230 \times 230\ \mu$m, which is divided into $1200 \times 300 \times 300$ cells along z, y and x direction respectively. Eight particles are initialized in each cell. Pre-ionized plasma is used and the profile of the plasma starts with a 19 μm linearly rising edge from $z = 127\ \mu$m, followed by a linear density up-ramp from 2.4 to 4×10^{17} cm^{-3} in 600 μm. This profile approximates the upper boundary of the grey region shown in figure 2(c). Two electron beam drivers with bi-Gaussian density profile are initialized, with a longitudinal length of $\sigma_z = 12.7\ \mu$m. The primary driver is asymmetric with scale lengths along the x and y directions of $\sigma_x = 14.4\ \mu$m and $\sigma_y = 18.2\ \mu$m. The secondary driver is symmetric with a radius of $\sigma_{x,y} = 14.4\ \mu$m. Here $\sigma_{x,y,z}$ represent the rms length of the electron beam in the corresponding directions. The separations between two drivers along x and y directions are 32 μm and 29 μm respectively, as shown in figure 4(d). The drivers propagate along the z direction and the probe propagates along the x direction. The probe used in this simulation is a 70 MeV, 8 fs (FWHM) electron beam without energy spread nor emittance. Figure 4(c) shows the simulated density modulation of the probe, which shows very similar features (including the phase shift) as observed in the experiment. This shows the capability of this new diagnostic tool to uncover more details about the wakefield structures which could be very helpful to understanding the physics.

2.3. Probing beam-driven wakes

Beam-driven PWFA is another attractive concept for high-energy-gain [8, 9] and high-efficiency acceleration [10, 16] of both electrons and positrons. Plasmas used in PWFA experiments usually have a much lower density ($\lesssim 10^{17}\mathrm{cm}^{-3}$) than that used in LWFA experiments, making it more challenging for optical methods to work. On the contrary, relativistic electron bunches generated from an LWFA can find their applicability for probing beam-driven wakes since the wakefields are still intense enough to deflect relativistic electrons. In this section, we show 3D PIC simulation results to illustrate the capability of the method we developed on visualizing such beam-driven wakes.

The simulation box has dimensions of $7860 \times 3140 \times 2360$ c/ω_0, which is divided into $1000 \times 400 \times 300$ cells along z, x and y directions respectively. Eight particles are initialized in each cell. Pre-ionized plasma is used and the profile of the plasma starts with a 50 c/ω_0 linearly rising edge from $z = 800$ c/ω_0, followed by a uniform density plasma with a peak density of $n_p = 6.4 \times 10^{-5} n_c$. The electron beam driver has a peak density of $n_b = 1.6 n_p$ and a bi-Gaussian density profile with rms length of $\sigma_z = 157$ c/ω_0 and rms width of $\sigma_{x,y} = 140$ c/ω_0. The driver is initially centred at $z = 400$ c/ω_0 and has an energy of 1 GeV without energy spread nor emittance. The probe used in this simulation is a 1 GeV, 7 fs (total length) electron beam without energy spread nor emittance for simplicity. The probe has a flat-top profile in x (propagation) direction and is uniform in the other two (transverse) directions. The peak density of the probe beam is $n_{\mathrm{probe}} = 1.5 \times 10^{-3} n_p$.

Figure 5(a) shows the plasma density distribution of the electron-beam-driven wake on the yz slice across the wake axis. The snapshot of the wake captured by the probe beam is shown in figure 5(b). The distance between the wake axis and the virtual screen where the snapshot is recorded is 2 mm. The drift length is limited to 2 mm in order to suppress probe electrons crossing from different plasma periods, otherwise, the snapshot will be blurred due to electrons crossing. This length can be increased by using a higher energy probe beam [42] because the deflecting angle of a higher energy electron induced by the wakefield is smaller, therefore the probe can drift a longer distance before the probe electrons crossing from different plasma periods happens. If the higher energy beam has a smaller divergence, to reach the same field of view, the distance between the source where the probe is generated and the wake that being probed should be changed accordingly to the change of the probe energy. From the snapshot in figure 5(b), one can immediately get much useful information on the wakefield that being probed, including the shape, dimensions and relative field strength. For example, the shape of the wake changes with $\xi = z - ct$, i.e., the first bubble has the sharpest sheath and slightly larger size than the following bubbles, as can be seen directly from the snapshot

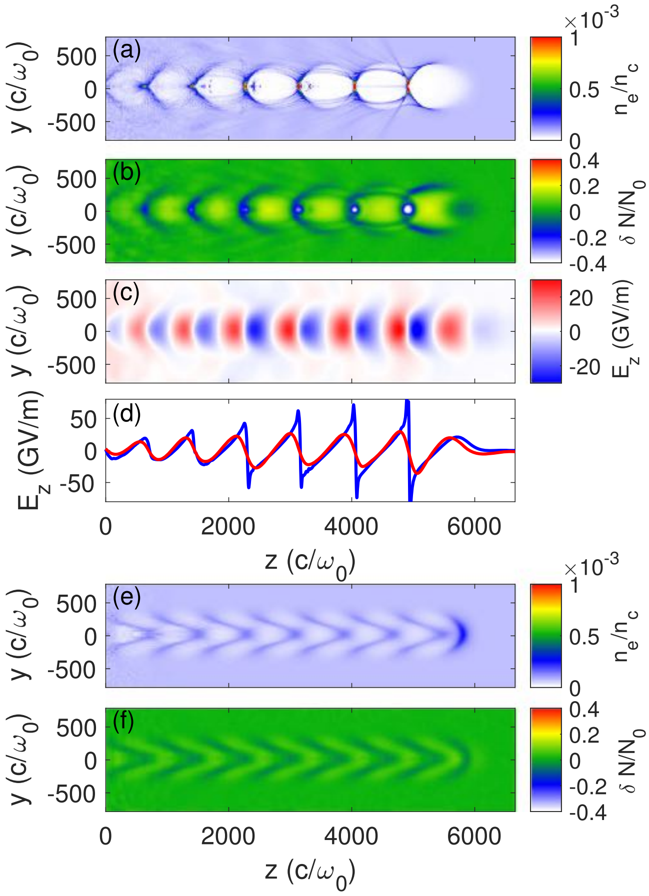

Figure 5. Snapshots of electron- and positron-driven wakes. (a) The plasma density on a slice across the wake axis obtained from simulation. (b) The simulated snapshot of the wake. (c) The reconstructed E_z field using the snapshot in (b). (d) Axial lineouts of the simulated (blue) and reconstructed (red) E_z field. (e) and (f) Plasma density and snapshot of a positron-driven wake.

in figure 5(b). The double-sheath structure of the second bubble can also be seen. The three holes sitting at the back of the first three bubbles represent that the electrons of the probe beam have been completely deflected by the extremely strong fields at these regions. Therefore, the relative size of these holes can give information on the relative strength of wakefields at these locations. Using the method described in [42], the wakefield can be reconstructed. In figures 5(c) and (d) we show the yz plot and the axial lineout of the reconstructed accelerating field E_z respectively. The blue line in figure 5(c) represents the E_z field obtained from the simulation, which shows a maximum accelerating gradient higher than 50 GV/m. The red line shows the reconstructed E_z field, which retrieves the low-frequency components of the simulated field. The reason for the loss of the high-frequency components is explained in detail in [42].

A positron beam can also be used to drive a wake [15, 16]. In figures 5(e) and (f), the plasma density distribution obtained from the PIC simulation and the snapshot of the wakefield are shown respectively. All the simulation parameters are the same except that the driver is replaced by a positron driver. Instead of expelling the plasma electrons outwards, the positron beam sucks the plasma electrons inwards, as a result, the wake structure is quite different from that driven by an electron beam. Nevertheless, the wakefield structure can still be captured by the probe beam very well as shown in figure 5(f). As the same in figure 5(b), the snapshot maps out the wakefield structure, therefore shows a density distribution being complementary to the density distribution of the wake itself, namely, the higher density region of the snapshot corresponds to the low-density region of the wake or vice versa. The field reconstruction method in [42] does not apply to the positron driven wake shown in figure 5(e) because the assumption that the wakefield has a Gaussian distribution in the transverse direction is violated. A more sophisticated model applicable to positron driven wakes will be a future work. We also note that the results of the positron-beam-driven wakes shown in figures 5(e) and (f) also apply to wakes driven by a proton beam with the same parameters.

3. Conclusion

Femtosecond relativistic electron bunches generated from a LWFA are used to probe the electric field structure of linear wakes driven by another synchronized laser in plasmas with different densities and density gradients. The spatiotemporal evolution of the wake in a plasma density up-ramp is recorded. Despite the fast-evolving feature of the wake, the initial profile of the low-density plasma upramp is reconstructed by analysing the measured wake wavelength. Parallel wakes excited by a laser with a main spot and sidelobes are identified from the snapshot captured by the probe beam. The capability of this new method for capturing the field structure of electron- and positron-driven wakes is also shown via 3D PIC simulations.

Acknowledgments

The authors wish to thank Dr Te-Sheng Hung, Mr Ying-Li Chang and Mr Yau-Hsin Hsieh for helping with these experiments. This work was supported by NSFC Grant No. 11425521, No. 11375006, No. 11535006, No. 11475101, the National Basic Research Program of China No. 2013CBA01501, the US DOE Grant No. DE-SC0010064, No. DE-SC0008491, No. DE-SC0008316, No. DE-SC0014260, the US NSF Grant PHY-1415386, No. ACI-1339893 and No. PHY-500630, and the Ministry of Science and Technology of Taiwan under Contracts No. 104-2112-M-001-030 MY3. Simulations are performed on Hoffman cluster at UCLA and Edison cluster at National Energy Research Scientific Computing Centre (NERSC).

ORCID iDs

C J Zhang https://orcid.org/0000-0001-8035-3014
F Li https://orcid.org/0000-0001-8627-910X

References

[1] Tajima T and Dawson J 1979 *Phys. Rev. Lett.* **43** 267–70
[2] Chen P, Dawson J, Huff R W and Katsouleas T 1985 *Phys. Rev. Lett.* **54** 693–6
[3] Rygg J *et al* 2008 *Science* **319** 1223–5
[4] Tabak M, Hammer J, Glinsky M E, Kruer W L, Wilks S C, Woodworth J, Campbell M E, Perry M D and Mason R J 1994 *Phys. Plasmas* **1** 1626–34
[5] Faure J, Glinec Y, Pukhov A, Kiselev S, Gordienko S, Lefebvre E, Rousseau J, Burgy F and Malka V 2004 *Nature* **431** 541–4
[6] Mangles S *et al* 2004 *Nature* **431** 535–8
[7] Geddes C, Toth C, Tilborg J, Esarey E, Schroeder C, Bruhwiler D, Nieter C, Cary J and Leemans W 2004 *Nature* **431** 538–41
[8] Hogan M *et al* 2005 *Phys. Rev. Lett.* **95** 054802
[9] Blumenfeld I *et al* 2007 *Nature* **445** 741–4
[10] Litos M *et al* 2014 *Nature* **515** 92–5
[11] Leemans W, Nagler B, Gonsalves A, Tóth C, Nakamura K, Geddes C, Esarey E, Schroeder C and Hooker S 2006 *Nat. Phys.* **2** 696–9
[12] Leemans W *et al* 2014 *Phys. Rev. Lett.* **113** 245002
[13] Kim H T, Pae K H, Cha H J, Kim I, Yu T J, Sung J H, Lee S K, Jeong T M and Lee J 2013 *Phys. Rev. Lett.* **111** 165002
[14] Wang X *et al* 2013 *Nat. Commun.* **4** 1988
[15] Blue B *et al* 2003 *Phys. Rev. Lett.* **90** 214801
[16] Corde S *et al* 2015 *Nature* **524** 442–5
[17] Lu W, Tzoufras M, Joshi C, Tsung F, Mori W B, Vieira J, Fonseca R and Silva L 2007 *Phys. Rev. Spec. Top.-Accel. Beams* **10** 061301
[18] Corde S, Phuoc T K, Lambert G, Fitour R, Malka V, Rousse A, Beck A and Lefebvre E 2013 *Rev. Mod. Phys.* **85** 1
[19] Esarey E, Schroeder C and Leemans W 2009 *Rev. Mod. Phys.* **81** 1229–85
[20] Schroeder C, Esarey E, Geddes C, Benedetti C and Leemans W 2010 *Phys. Rev. Spec. Top.-Accel. Beams* **13** 101301
[21] Malka V, Faure J, Gauduel Y A, Lefebvre E, Rousse A and Phuoc K 2008 *Nat. Phys.* **4** 447–53
[22] Joshi C and Katsouleas T 2003 *Phys. Today* **56** 47–53
[23] Suk H, Barov N, Rosenzweig J and Esarey E 2001 *Phys. Rev. Lett.* **86** 1011–4
[24] Buck A *et al* 2013 *Phys. Rev. Lett.* **110** 185006
[25] Xu X L, Li F, An W, Dalichaouch T N, Yu P, Lu W, Joshi C and Mori W B 2017 *Phys. Rev. Accel. Beams* **20** 111303
[26] Katsouleas S, Wilks T, Dawson J M and Su J J 1987 *Part. Accel.* **22** 81–99
[27] Tzoufras M, Lu W, Tsung F, Huang C, Mori W B, Katsouleas T, Vieira J, Fonseca R and Silva L 2008 *Phys. Rev. Lett.* **101** 145002
[28] Vafaei-Najafabadi N *et al* 2008 *Phys. Rev. Lett.* **112** 025001
[29] Couperus J *et al* 2017 *Nat. Commun.* **8** 487
[30] Centurion M, Reckenthaeler P, Trushin S, Krausz F and Fill E 2008 *Nat. Photon.* **2** 315–8
[31] Schumaker W *et al* 2013 *Phys. Rev. Lett.* **110** 015003
[32] Li C, Séguin F, Frenje J and Rosenberg M 2010 *Science* **327** 1231–5
[33] Clayton C E *et al* 2016 *Nat. Commun.* **7** 12483
[34] Zhang C J *et al* 2017 *Phys. Rev. Lett.* **119** 064801
[35] Matlis N *et al* 2006 *Nat. Phys.* **2** 749–53
[36] Li Z *et al* 2014 *Nat. Commun.* **5** 3085
[37] Buck A, Nicolai M, Schmid K, Sears C M, Sävert A, Mikhailova J M, Krausz F, Kaluza M C and Veisz L 2011 *Nat. Phys.* **7** 543–8
[38] Sävert A *et al* 2015 *Phys. Rev. Lett.* **115** 055002
[39] Lundh O *et al* 2011 *Nat. Phys.* **7** 219–22
[40] Zhang C J *et al* 2016 *Phys. Rev. Accel. Beams* **19** 062802

[41] Tilborg J, Schroeder C, Filip C, Tóth C, Geddes C, Fubiani G, Huber R, Kaindl R, Esarey E and Leemans W 2006 *Phys. Rev. Lett.* **96** 014801
[42] Zhang C J *et al* 2016 *Sci. Rep.* **6** 29485
[43] Panofsky W and Wenzel W A 1956 *Rev. Sci. Instrum.* **27** 967
[44] Zhang C J, Joshi C, Xu X, Mori W B, Li F, Wan Y, Hua J, Pai C, Wang J and Lu W 2018 *Plasma Phys. Control. Fusion* **60** 024003
[45] Wen M, Shen B, Zhang X, Ji L, Wang W, Xu J and Yu Y 2010 *Phys. Plasmas* **17** 103113